Creation and Recombination of Frenkel Defects in AgBr

K. Funke[a], T. Lauxtermann[a], D. Wilmer[a], and S. M. Bennington[b]

[a] Institut für Physikalische Chemie, Schlossplatz 4/7, D-48149 Münster
[b] Rutherford Appleton Laboratory, Chilton, Oxfordshire OX11 0QX, U.K.

Z. Naturforsch. **50a**, 509–520 (1995); received November 14, 1994

Dedicated to Professor Ewald Wicke on the occasion of his 80th birthday

Complete ionic conductivity spectra as well as quasielastic and inelastic neutron scattering spectra have been taken of solid silver bromide at various temperatures. High-amplitude vibrational movements, essentially of the silver ions, contribute to both kinds of spectra. In particular, a conductivity maximum, located at about 500 GHz, reflects oscillations of individual silver ions along ⟨111⟩ directions. – The microwave and millimetre-wave conductivities are dominated by a thermally activated Debye-type relaxation process. The effect is consistently explained by the frequent hopping of silver ions from regular octahedral lattice sites into tetrahedral interstitial sites and back again, i.e., by the frequent creation and recombination of Frenkel pairs. – The effect is also responsible for the existence of thermally activated quasielastic components in the neutron scattering spectra. The width of the coherent quasielastic scattering shows that the forward-backward hopping of a silver ion is accompanied by fast correlated movements of ions in its immediate neighbourhood.

I. Introduction

Silver bromide, AgBr, is one of the most thoroughly studied solid electrolytes, see for instance [1]. It is a fast ionic conductor at temperatures well below its melting point, with a conductivity of 0.1 $\Omega^{-1}\,cm^{-1}$ at about 625 K [2–4]. The cation mobility in AgBr is caused by the thermally activated formation of Frenkel defects in the rocksalt structure, the Frenkel-pair formation enthalpy being about 1.15 eV [5, 6]. On the basis of temperature dependent conductivity and tracer diffusion data as well as model calculations, various migration enthalpies have been derived, the lowest applying to the collinear interstitialcy mechanism [7, 8].

In 1961 Everett et al. [9] published microwave conductivity data of AgBr, taken at 23 GHz. The conductivity was found to be significantly larger at 23 GHz than at 1 kHz [2–4], and the effect was attributed to a Debye-Falkenhagen type of relaxation [10, 11] of the mobile silver ions. In an effort to substantiate the findings of Everett et al. we have performed conductivity measurements in a broad frequency range. While our earlier data were restricted to frequencies below 60 GHz [12], we now present complete conductivity spectra which also comprise the millimetre-wave and far-infrared frequency regimes, up to 10 THz. Our data corroborate the existence of a pronounced conductivity dispersion at microwave frequencies. However, as already stated in [12], they clearly do not bear the distinguishing marks of a Debye-Falkenhagen-type jump relaxation process; these would include a power law frequency dependence of the conductivity with an exponent of less than one, see, e.g., [13, 14]. Instead, the observed frequency-dependent conductivity seems to follow a power law with an exponent of two, which is typical of an ordinary Debye relaxation in a rigid double-well or multi-well potential. In [12] we suggested that the effect should be explained in terms of the frequent hopping of silver ions from their regular octahedral lattices sites into tetrahedral interstitial sites and back again, i.e., by the frequent creation and recombination of Frenkel pairs. This interpretation would be in agreement with structural data showing significant silver-ion probability density between lattice sites and interstitial sites [15–17].

Our present measurements include angular frequencies that are of the order of, and even larger than, the inverse time constant of the Debye-type process. In fact, the numerical value of this time constant has been unknown up to now. Moreover, we also observe high-amplitude vibrations of individual silver ions along ⟨111⟩ directions. The information that is now available enables us to give a more complete description of the silver-ion dynamics than in [12], while the basic statement concerning the creation and recombination of Frenkel pairs remains unchanged.

The conductivity data led us to believe that the effect should also be visible in quasielastic neutron

Reprint requests to Prof. Dr. K. Funke.

0932-0784 / 95 / 0600-0509 $ 06.00 © – Verlag der Zeitschrift für Naturforschung, D-72027 Tübingen

scattering spectra. The respective experiment has been performed on the time-of-flight spectrometer MARI at the British spallation source ISIS, and a thermally activated quasielastic component has, indeed, been detected.

Some experimental details are described in Sect. II, while Sect. III and IV are devoted to our conductivity and neutron-scattering results, respectively. Interestingly, these results turn out not to be redundant but complementary, as the two techniques provide a different weighing of components due to non-periodic processes occurring on different length scales. In particular, the width of the coherent quasielastic scattering reflects the existence of fast cooperative movements of neighbouring ions while the *central* silver ion performs its trial-and-error hopping sequence. This will be discussed in Sect. IV, and a conclusion will be given in Section V.

II. Experimental

II.1 Dynamic Conductivity

Complete conductivity spectra of AgBr have been taken at temperatures between 448 K and 623 K. Various experimental setups were applied to cover the frequency range from 4 MHz to 10 THz. All setups use a common principle: the electrical conductivity is derived from the transmission and/or reflexion behaviour of the sample with respect to an incoming electromagnetic wave. The conductivity at the respective frequency can be determined with the help of the continuity conditions for the electromagnetic field at the sample/air phase boundaries.

The employed techniques can be divided into two groups:

(i) microwave spectroscopy. From 4 MHz to 105 GHz, coaxial and rectangular waveguide systems have been utilized. For the measurements, a short waveguide section was filled with silver bromide. Up to 2.6 GHz, we determined the amplitudes and phases of transmitted waves; at higher frequencies, we measured the amplitudes of transmitted and/or reflected waves. Further details regarding data acquisition and analysis can be found elsewhere [18–20].
All samples were prepared from the melt. Special care was taken to produce exact sample geometries and to provide good electrical contact to the waveguide. The whole sample preparation was performed under dark-room conditions.

(ii) FTIR spectroscopy. A BOMEM DA8.1 Fourier transform spectrometer was used in the FIR regime, at frequencies between 240 GHz and 10 THz. A mercury lamp served as radiation source for a Michelson interferometer; the light transmitted by thin (80 μm to 200 μm) AgBr samples, prepared from the melt and mechanically reduced to their requisite sizes, was detected by a helium-cooled silicon bolometer (Infrared Labs.) as a function of the optical path difference given by the moving-mirror displacement. The interferograms were then Fourier-transformed to give the transmission spectra which were further analyzed by a procedure similar to that used in microwave spectroscopy [18–20].

II.2 Quasielastic Neutron Scattering

The dynamic structure factor of AgBr has been measured on the direct-geometry time-of-flight spectrometer MARI at the spallation neutron source ISIS, located at the Rutherford Appleton Laboratory, Didcot, England.

Hollow cylindrical AgBr (99.9%, Johnson Matthey) powder samples of approximately 3 mm thickness were mounted in a thin-wall (250 μm) Niobium container which simultaneously served as an electric oven. A housing of several Niobium heat shields assured temperature constancy during the different runs.

Measurements were performed at three temperatures (423 K, 548 K, 623 K) using thermal neutrons of 20 meV incident energy. The energy resolution was 0.2 meV.

Data correction and transformation of the time-of-flight data to $S(Q, \omega)$ were performed using the Speal/Squeal program package available on MARI.

III. Conductivity Spectra and Their Interpretation

In Fig. 1 we present a typical ionic conductivity spectrum of AgBr, taken at 473 K and covering the frequency range from 10^9 Hz to 10^{13} Hz. On the low-frequency side, the data reach the dc value of the conductivity. At comparatively high frequencies, above 10^{12} Hz, we observe a pronounced conductivity maximum, which is due to the excitation of transverse optical phonons. The more interesting features of the

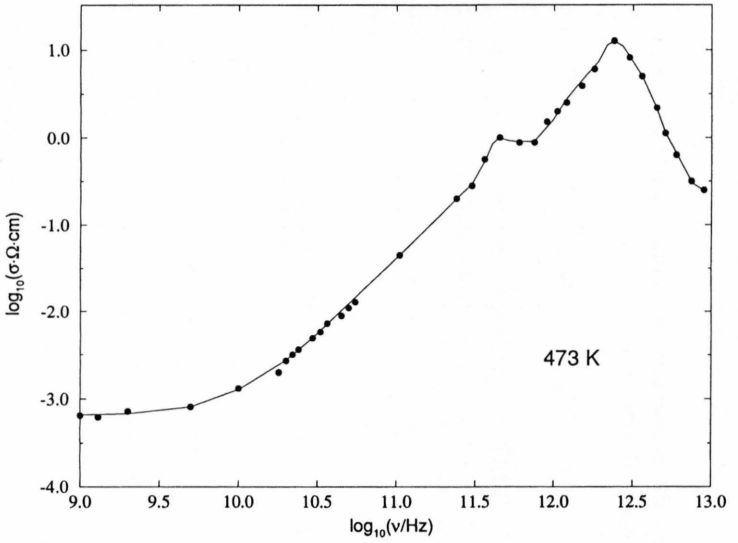

Fig. 1. Frequency dependent electrical conductivity of AgBr at 473 K, from 1 GHz to 10 THz.

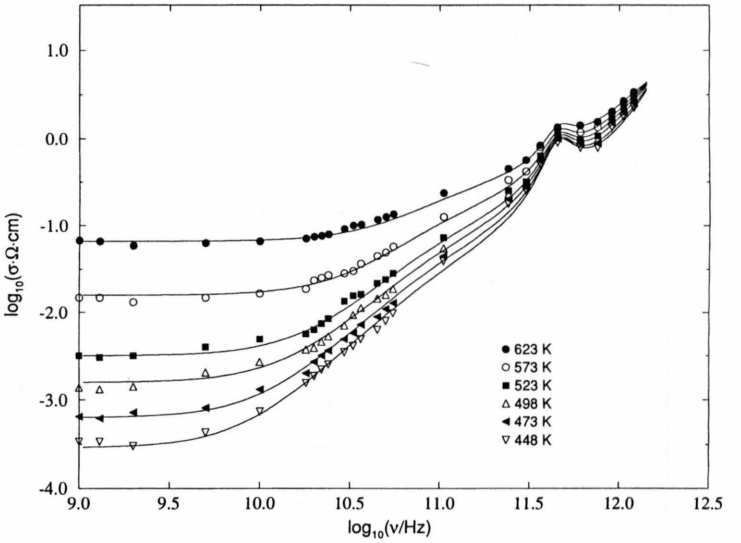

Fig. 2. Frequency dependent electrical conductivity of AgBr at six temperatures. The solid lines result from the fit described in the text.

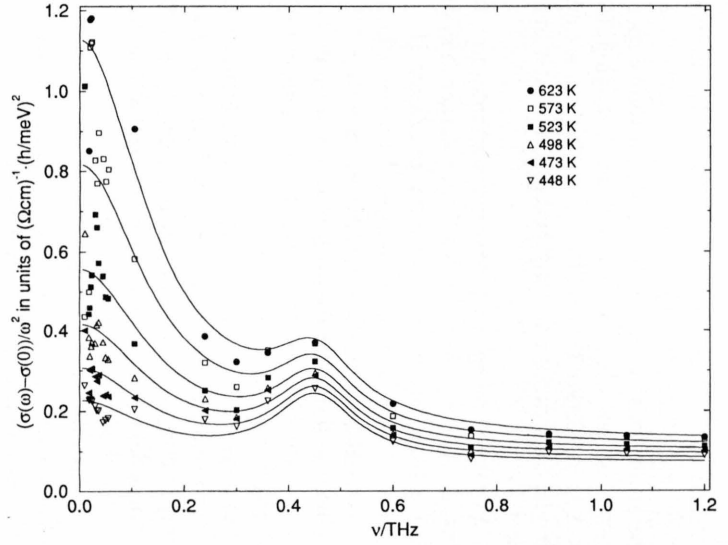

Fig. 4. The data of Fig. 2, replotted as $(\sigma(\omega)-\sigma(0))/\omega^2$. The solid lines correspond to those of Figure 2.

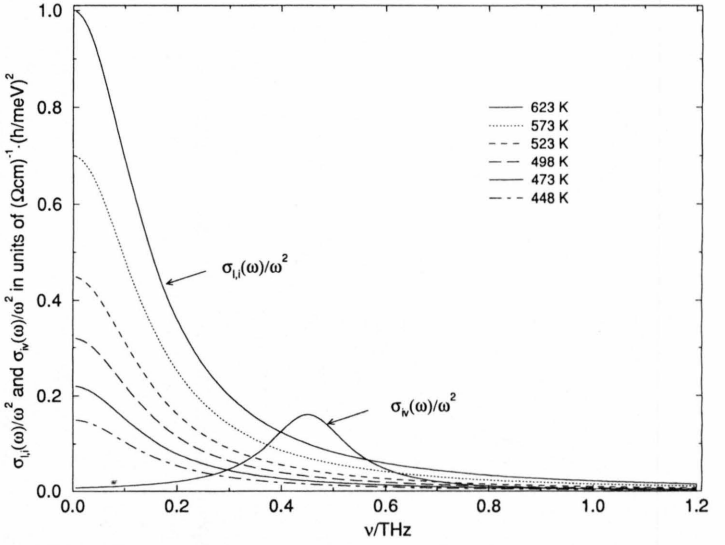

Fig. 5. The Lorentzian functions $\sigma_{l,i}(\omega)/\omega^2$, see (11), and $\sigma_{iw}(\omega)/\omega^2$, see (13) and (17), as employed for the construction of the solid lines of Figs. 2 and 4.

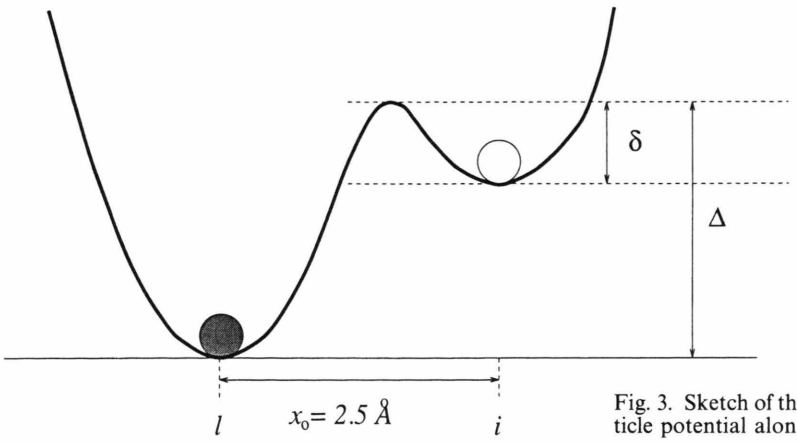

Fig. 3. Sketch of the ansatz used for the silver-ion single-particle potential along ⟨111⟩ directions.

spectrum are, however, located at intermediate frequencies, i.e., roughly between 10^{10} Hz and 10^{12} Hz. Two particular phenomena show up in this part of the spectrum:

(i) For about one decade on the frequency scale, say, from 20 to 200 GHz, the conductivity follows a power law with an exponent close to two.
(ii) At frequencies between about 300 and 700 GHz we observe an additional maximum of the conductivity.

Interestingly, feature (i) turns out to be thermally activated, while (ii) hardly seems to change with temperature. This is seen in Fig. 2 which shows spectra taken at six different temperatures, ranging from 448 K to 623 K. The solid lines result from a simple model construction and will be explained later in this section.

In the following, let us first focus attention on feature (i). As the power-law exponent is larger than one, any explanation in terms of jump relaxation [13, 14] can be excluded beforehand. Instead, the contribution to the conductivity that is superimposed onto its dc value is *well* described by a power law with an exponent of two. This is the typical feature of an ordinary Debye relaxation process.

In a system of hopping ions, a simple Debye relaxation is indicative of a localized back-and-forth hopping in a rigid potential. In AgBr, hops of silver ions from ordinary octahedral lattice sites (l) into interstitial tetrahedral sites (i) and back again are the only candidates for such a process. In fact, simple energetic arguments show that a vacancy-interstitial-ion pair will recombine in a vast majority of cases, see below. Inversely, the interstitial ion will only rarely be liberated from the vacancy, forming a lasting Frenkel pair.

Figure 3 is a sketch of the (rigid) single-particle potential of the hopping silver ion. The energy barriers for l to i and i to l hops are denoted by Δ and δ, respectively. The mutual distance of l and i is roughly 2.5 Å.

For our discussion of the hopping dynamics, let us first consider the mean residence times for the ion at l and i:

$$\tau_l = \tau_{l0} \cdot \exp(\Delta/kT) \quad \text{and}$$
$$\tau_i = \tau_{i0} \cdot \exp(\delta/kT)\,. \tag{1}$$

Then, the probability of finding the ion at l, W_l, will change with time at a rate given by

$$\dot{W}_l(t) = \frac{1}{\tau_i} W_i(t) - \frac{1}{\tau_l} W_l(t)\,. \tag{2}$$

In (2), $W_i(t)$ is the time dependent probability for finding the ion at i. For convenience, a relaxation time τ is introduced by

$$\frac{1}{\tau} = \frac{1}{\tau_i} + \frac{1}{\tau_l}\,. \tag{3}$$

Because of the identity $W_i(t) + W_l(t) \equiv 1$, (2) and the corresponding expression for $\dot{W}_i(t)$ are now rewritten as

$$\dot{W}_l(t) = \frac{1}{\tau_i} - \frac{1}{\tau} W_l(t) \quad \text{and}$$
$$\dot{W}_i(t) = \frac{1}{\tau_l} - \frac{1}{\tau} W_i(t)\,. \tag{4}$$

Suppose the ion hops from l to i at time 0. At later times t, the probability $W_l(t)$ and the backhop rate,

$\dot{W}_l(t)$, are then

$$W_l(t) = \frac{\tau}{\tau_i}(1 - e^{-t/\tau}) \text{ and } \dot{W}_l(t) = \frac{1}{\tau_i} e^{-t/\tau}. \quad (5)$$

Similarly, a hop from i to l at time 0 results in a backhop rate at later times t which is given by

$$\dot{W}_i(t) = \frac{1}{\tau_l} e^{-t/\tau}. \quad (6)$$

For constructing the frequency dependent conductivity due to the hopping between l and i, we need to know the velocity autocorrelation function for this hopping, $\langle \boldsymbol{v}(0) \cdot \boldsymbol{v}(t) \rangle_{l,i}$. There are four contributions to this function,

$$\langle \boldsymbol{v}(0) \cdot \boldsymbol{v}(t) \rangle_{l,i} \propto \left\{ \frac{\delta(t)}{2} - \frac{1}{\tau_i} e^{-t/\tau} \right\} + \left\{ \frac{\delta(t)}{2} - \frac{1}{\tau_l} e^{-t/\tau} \right\}, \quad (7)$$

representing the correlations of an l to i hop with itself and with a backward hop at a later time, see the first pair of braces, and the respective correlations in the other direction, see the second pair of braces. In (7), $\delta(t)$ is the delta function. Note that effects resulting from a finite duration of a hop have not been included in (7). This would require substitution of functions of finite width for the delta functions and would result in a conductivity which decreases at high frequencies instead of staying constant. At high frequencies, however, the experimental conductivities are no longer dominated by the l, i hopping, but by vibrational contributions. The error made in writing (7) is, therefore, negligible. We thus have

$$\langle \boldsymbol{v}(0) \cdot \boldsymbol{v}(t) \rangle_{l,i} = \left\{ \delta(t) - \frac{1}{\tau} e^{-t/\tau} \right\} \cdot \frac{x_0^2}{\tau_l + \tau_i}. \quad (8)$$

Besides the hopping distance, $x_0 \approx 2.5$ Å, (8) contains the average rate of two consecutive hops, $1/(\tau_l + \tau_i)$.

According to linear response theory [21], a Fourier transformation relates $\langle \boldsymbol{v}(0) \cdot \boldsymbol{v}(t) \rangle_{l,i}$ to the corresponding conductivity component, $\sigma_{l,i}$, provided the l, i hopping of different silver ions is uncorrelated. This is, however, a very reasonable assumption. Therefore, $\sigma_{l,i}(\omega)$ should be given by

$$\sigma_{l,i}(\omega) = \frac{ne^2}{3kT} \int_{0^-}^{\infty} \langle \boldsymbol{v}(0) \cdot \boldsymbol{v}(t) \rangle_{l,i} \cos(\omega t) \, dt = \frac{ne^2}{3kT} \cdot \frac{x_0^2}{\tau_l + \tau_i} \cdot \frac{\omega^2 \tau^2}{1 + \omega^2 \tau^2}. \quad (9)$$

In (9), n is the Ag^+ number density and e the elementary charge. We have at all temperatures

$$\tau_i \ll \tau_l, \quad (10)$$

as is immediately apparent from a parameterization like that based on Fig. 4, see below. Therefore, τ and τ_i are virtually identical, and (9) is rewritten in the following way:

$$\frac{\sigma_{l,i}(\omega)}{\omega^2} = \frac{ne^2}{3kT} \cdot x_0^2 \cdot \frac{\tau_i^2}{\tau_l} \cdot \frac{1}{1 + \omega^2 \tau_i^2}. \quad (11)$$

The function $\sigma_{l,i}(\omega)/\omega^2$ is, hence, expected to be a Lorentzian. The two unknown quantities, τ_i and τ_l, are most conveniently read from its width and weight.

For comparison with (11), the experimental data of Fig. 2 are now replotted as $(\sigma(\omega) - \sigma(0))/\omega^2$, see Figure 4. The expected Lorentzians clearly show up in this figure. Their weight increases with increasing temperature, while their width appears to stay rather constant. This implies that $1/\tau_l$ is thermally activated, while the activation energy for the hop from i to l is negligible. With regard to Fig. 3 this means that the single-particle potential has, in fact, not a minimum, but a saddle-point at site i.

The numerical fits of Figs. 2 and 4 have been achieved by considering four contributions to the conductivity:

$$\sigma(\omega) = \sigma(0) + \sigma_{l,i}(\omega) + \sigma_{iv}(\omega) + \sigma_{ph}(\omega). \quad (12)$$

Here, the third and fourth contributions are due to particular individual vibrational movements of the silver ions and to transverse optical phonons, respectively. Note that at frequencies of the order of the inverse duration of a hop, and above, (12) is a reasonable approximation only as long as $\sigma_{iv}(\omega) + \sigma_{ph}(\omega)$ is much larger than $\sigma(0) + \sigma_{l,i}(\omega)$. In the frequency range of Figs. 2 and 4, this is, however, guaranteed.

The last term of (12) is particularly simple, as the low-frequency flank of the phonon-type vibrational contributions increases as ω^2 at all temperatures. Therefore, this term provides only a constant (but slightly temperature dependent) background in the plot of Figure 4.

As soon as $\sigma_{l,i}(\omega)/\omega^2$ and $\sigma_{ph}(\omega)/\omega^2$ are identified in the spectra of Fig. 4, the remaining term, $\sigma_{iv}(\omega)/\omega^2$, may be considered. It does not seem to have any detectable temperature dependence and is well fitted by a Lorentzian centred at the angular frequency of its maximum, ω_{iv}, its half width at half maximum

(HWHM) on the angular frequency scale being $1/\tau_{iv}$:

$$\frac{\sigma_{iv}(\omega)}{\omega^2} \propto \frac{1}{1+(\omega-\omega_{iv})^2\,\tau_{iv}^2}. \tag{13}$$

Our experimental data of Fig. 4 are best fitted, if $\sigma_{l,i}(\omega)/\omega^2$ and $\sigma_{iv}(\omega)/\omega^2$ are represented by the Lorentzians shown in Figure 5. Here, only the weight of $\sigma_{l,i}(\omega)/\omega^2$ is temperature dependent, while its width as well as both weight and width of $\sigma_{iv}(\omega)/\omega^2$ do not depend on temperature.

Before revisiting the l,i hopping motion of the silver ions, let us briefly consider the meaning of the term $\sigma_{iv}(\omega)$, which was denoted (ii) at the beginning of this section. It is important to realize that $\sigma_{iv}(\omega)$ is not caused by the excitation of phonons in AgBr. The reason for this is not the absence of an oscillatory dipole moment in transverse acoustic phonon modes. In fact, differences in the vibrational amplitudes of cations and anions will create oscillating dipole moments. Rather, the reason is that our measurement is restricted to the centre of the Brillouin zone. Because of its small momentum, a quantum of far-infrared light is unable to excite any low-frequency mode of motion that is spatially periodic. On the other hand, the frequencies of transverse *optical* phonons at the centre of the Brillouin zone are known to be much larger [22], in agreement with the conductivity maximum observed beyond 1 THz, cf. Figure 1. Therefore, $\sigma_{iv}(\omega)$ has to be due to some spatially non-periodic vibrational motion of individual ions.

This feature, together with the particularly low value of ω_{iv}, is best understood in terms of high-amplitude oscillations of individual silver ions, performed in those directions where their anisotropic single-particle potentials are especially wide. Evidently, these are the $\langle 111\rangle$ directions, towards the interstitial sites. The shape of the silver-ion single-particle potential at site l, along $\langle 111\rangle$, is thus tentatively described by

$$V(x) = \frac{1}{2}\, m_{Ag} \cdot \omega_{iv}^2 \cdot x^2. \tag{14}$$

Here m_{Ag} is the mass of a silver ion. In fact, (14) agrees very well with the numerical value of the barrier height for l to i hops, Δ, see below.

In the following, let us assume that at a given instant of time only a fraction ξ of all silver ions perform a high-amplitude vibrational motion along one of the $\langle 111\rangle$ directions, and that these oscillations of individual ions are uncorrelated. Their mean square displacement due to this kind of motion, $\langle r^2(t)\rangle_{iv}$, is then related to $\sigma_{iv}(\omega)$ via [14, 23]

$$\sigma_{iv}(\omega) = \xi \cdot \frac{n e^2}{3kT} \cdot \mathrm{Re}\left\{\lim_{\varepsilon\to 0}(\varepsilon+i\omega)^2 \cdot \int_0^\infty \langle r^2(t)\rangle_{iv} \cdot e^{-(\varepsilon+i\omega)t}\,\mathrm{d}t\right\}. \tag{15}$$

Inserting

$$\langle r^2(t)\rangle_{iv} = \langle r^2(\infty)\rangle_{iv}\left\{1-\cos(\omega_{iv}t)\cdot e^{-t/\tau_{iv}}\right\} \tag{16}$$

we find

$$\sigma_{iv}(\omega) = \xi \cdot \frac{n e^2}{3kT} \cdot \langle r^2(\infty)\rangle_{iv} \cdot \frac{\omega^2\tau_{iv}}{1+(\omega-\omega_{iv})^2\cdot\tau_{iv}^2}, \tag{17}$$

in agreement with (13). The numerical values of ω_{iv} and τ_{iv} being 2.8 ps^{-1} and 1.65 ps, respectively, the normalized mean square displacement, $\langle r^2(t)\rangle_{iv}/\langle r^2(\infty)\rangle_{iv}$, is now readily obtained from (16). Figure 6 is a plot of this function.

Compared with the entire vibrational energy per ion, which is about $3kT$, the energy contained in feature (ii) per ion is only a small fraction. This is seen when $\xi\cdot(m_{Ag}/2)\cdot\langle \boldsymbol{v}(0)\cdot\boldsymbol{v}(0)\rangle_{iv}$ is formed using the relation

$$\langle \boldsymbol{v}(0)\cdot\boldsymbol{v}(0)\rangle_{iv} = \frac{1}{2}\frac{\mathrm{d}^2}{\mathrm{d}t^2}\langle r^2(t)\rangle_{t=0} = \frac{1}{2}\,\omega_{iv}^2\cdot\langle r^2(\infty)\rangle_{iv}. \tag{18}$$

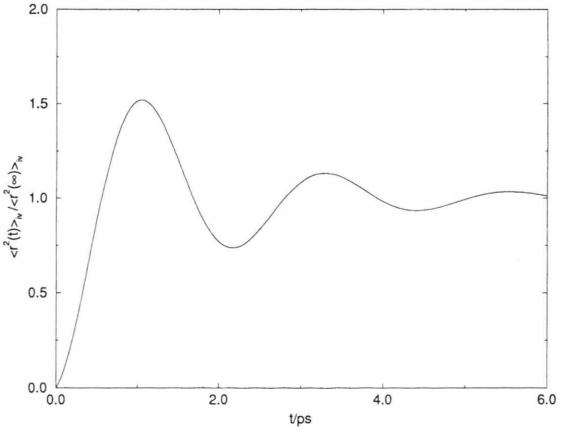

Fig. 6. Normalized time dependent mean square displacement of the individual vibrational movement, cf. (16).

Taking $\xi \cdot \langle r^2(\infty)\rangle_{iv}$ from (17), we find that the ratio

$$\frac{\xi \cdot (m_{Ag}/2) \cdot \langle v(0) \cdot v(0)\rangle_{iv}}{3kT} = \frac{m_{Ag} \cdot \sigma_{iv}(\omega_{iv})}{4ne^2 \cdot \tau_{iv}} \qquad (19)$$

is only about 0.003 and temperature independent. The temperature independence shows that the observed vibrational motion is not performed by interstitial ions and is, moreover, not influenced by the degree of disorder. Most probably, the ratio of (19) is so small as ξ is small. The reason for this is seen in the geometrical restrictions imposed by the pronounced anisotropy of the silver-ion potential at an ordinary lattice site. This is at the same time a plausible explanation for the lack of spatial periodicity of this particular kind of oscillations.

Let us now return to the l, i hopping motion, which causes the central components in Figures 4 and 5. Fits according to (11) show that the mean residence time at an interstitial site, τ_i, has to be about 1 ps at all temperatures, implying a negligible backward barrier height, δ. On the other hand, the mean residence time τ_l is much longer, see Figure 7. Interestingly, the apparent activation energy for $1/\tau_l$ seems to decrease as the temperature increases. A corresponding trend was observed earlier for the formation enthalpies of lasting Frenkel pairs in AgBr and AgCl [24]. The activation energy Δ read from Fig. 7 within the linear low-temperature regime is about 0.29 eV. This is much less than the formation enthalpy for a lasting Frenkel pair, $\Delta_{\text{Frenkel}} \approx 1.15$ eV. A relatively large additional amount of energy is, therefore, required to liberate the interstitial ion from the vacancy, which acts as a Coulomb trap:

$$\Delta_{\text{lib}} = \Delta_{\text{Frenkel}} - \Delta \approx 0.86 \text{ eV}. \qquad (20)$$

This is sketched in Figure 8. Note that the shape of the potential of (14) which has been used in Fig. 8 around site l, in the l to i direction, agrees very well with $\Delta \approx 0.29$ eV.

The liberation energy, Δ_{lib}, is several times the thermal energy, while the backward barrier height, δ, is negligible. This explains why an l to i hop is virtually always followed by the backward hop from i to l and thus justifies the Debye-type ansatz made in the beginning of this section.

The liberation energy is the difference in energy experienced by an interstitial silver ion with and without a vacancy as its nearest neighbour. For an electrostatic estimate, we note

$$\Delta_{\text{lib}} > \frac{e^2}{4\pi\varepsilon_0\,\varepsilon(\infty)\,x_0} \approx 0.4 \text{ eV}. \qquad (21)$$

Here we have inserted our experimental high-frequency value of the permittivity, $\varepsilon(\infty)$. From 473 K to 573 K these values vary from 14.8 ± 0.2 to 17.2 ± 0.2. In (21), the reason why Δ_{lib} is still considerably larger than 0.4 eV is the following. The interstitial ion, the vacancy it left behind, and the entire neighbourhood will be geometrically relaxed towards each other, lowering the potential energy of this configuration. This rather static view is in agreement with a more dynamic result to be obtained in the next section, viz., the observation of fast displacive movements of the neighbouring ions which are correlated with the forward-backward hopping sequence of the *central* silver ion.

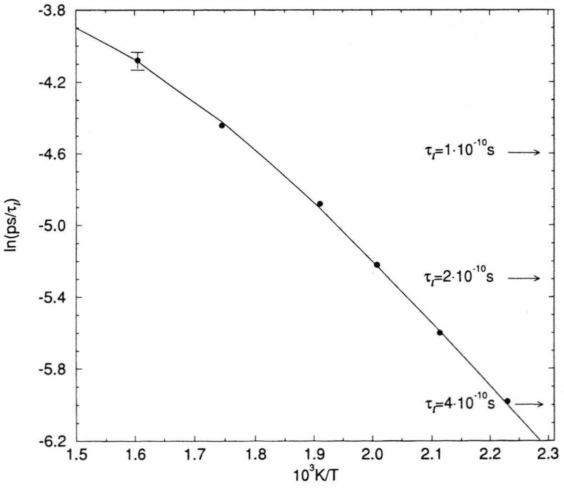

Fig. 7. Arrhenius plot of the inverse mean residence time of a silver ion at a lattice site.

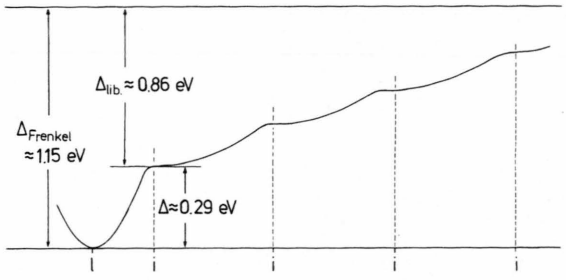

Fig. 8. Schematic plot of the potential experienced by a silver ion. Close to lattice site l, (14) has been used; Δ is the activation energy obtained from Figure 7. Note that the plot is extremely schematic beyond the first interstitial site. The arrangement of sites l, i, i is *not* linear, and further Ag^+ transport is via the collinear interstitialcy mechanism.

IV. Neutron Scattering Spectra and Their Interpretation

Correlated forward-backward hopping sequences like those detected in AgBr are non-periodic dynamic processes and will, therefore, contribute quasielastic intensity to energy-resolved neutron scattering spectra.

In the following, we will first adhere to the rather simplistic view of the hopping dynamics that was developed in the preceding section and use it as a basis to describe the expected quasielastic scattering. In a second step, we will compare our expectations with the actual quasielastic contributions to the neutron-scattering spectra. This will, thirdly, necessitate a refinement of our view in the sense that the hopping of the *central* ion is accompanied by correlated movements of its neighbours.

Total neutron scattering spectra of powder samples of AgBr will generally consist of the following six constituent parts:

$$\begin{aligned} S^{\mathrm{tot}}(Q,\omega) = {} & \sigma_{\mathrm{inc}}^{\mathrm{Ag}} S_{\mathrm{inc}}^{\mathrm{Ag}}(Q,\omega) + \sigma_{\mathrm{coh}}^{\mathrm{Ag}} S^{\mathrm{AgAg}}(Q,\omega) \\ & + \sqrt{\sigma_{\mathrm{coh}}^{\mathrm{Ag}} \sigma_{\mathrm{coh}}^{\mathrm{Br}}}\,[S^{\mathrm{AgBr}}(Q,\omega) + S^{\mathrm{BrAg}}(Q,\omega)] \\ & + \sigma_{\mathrm{coh}}^{\mathrm{Br}} S^{\mathrm{BrBr}}(Q,\omega) + \sigma_{\mathrm{inc}}^{\mathrm{Br}} S_{\mathrm{inc}}^{\mathrm{Br}}(Q,\omega)\,. \end{aligned} \tag{22}$$

The numerical values of the scattering cross sections are [25]:

$$\sigma_{\mathrm{inc}}^{\mathrm{Ag}} = 0.58 \text{ barn}, \quad \sigma_{\mathrm{coh}}^{\mathrm{Ag}} = 4.41 \text{ barn}$$
$$\sigma_{\mathrm{inc}}^{\mathrm{Br}} = 0.10 \text{ barn}, \quad \sigma_{\mathrm{coh}}^{\mathrm{Br}} = 5.79 \text{ barn}\,.$$

In our experiment, we have avoided any Bragg scattering by our sample and its environments. As a consequence, we are restricted to a narrow range of Q values around 3.4 Å^{-1}.

Starting out with our simplistic view, we now assume that the only hopping or non-periodic displacive motion in the system is performed by individual silver ions, between sites l and i, as described in Section III. As Bragg scattering has been avoided, there is only little elastic scattering in the spectra. It is partly coherent, due to the disorder, and partly incoherent, due to the bromide ions. The incoherent silver scattering, however, will be quasielastic. Of course, the same holds true for the self-part of the coherent silver scattering. We, therefore, expect the quasielastic component to be proportional to that of $S_{\mathrm{inc}}^{\mathrm{Ag}}(Q,\omega)$. The latter function is the directional average of $S_{\mathrm{inc}}^{\mathrm{Ag}}(\boldsymbol{Q},\omega)$, which is itself related to the van-Hove self-correlation function of the silver ions, $G_{\mathrm{s}}^{\mathrm{Ag}}(\boldsymbol{r},t)$, via Fourier transformations in both space and time.

To formulate the function $G_{\mathrm{s}}^{\mathrm{Ag}}(\boldsymbol{r},t)$ pertinent to the l,i hopping, let us reconsider Figure 3. The *a priori* probabilities for finding the silver ion at sites l and i are τ/τ_i and τ/τ_l, respectively. $G_{\mathrm{s}}^{\mathrm{Ag}}(\boldsymbol{r},t)$ will then consist of four parts:

$$\begin{aligned} G_{\mathrm{s}}^{\mathrm{Ag}}(\boldsymbol{r},t) = {} & \delta(\boldsymbol{r})\cdot\frac{\tau}{\tau_i}\left[1-\frac{\tau}{\tau_l}(1-e^{-t/\tau})\right] \\ & + \delta(\boldsymbol{r}-\boldsymbol{x}_0)\cdot\frac{\tau}{\tau_i}\left[\frac{\tau}{\tau_l}(1-e^{-t/\tau})\right] \\ & + \delta(\boldsymbol{r})\cdot\frac{\tau}{\tau_l}\left[1-\frac{\tau}{\tau_i}(1-e^{-t/\tau})\right] \\ & + \delta(\boldsymbol{r}+\boldsymbol{x}_0)\cdot\frac{\tau}{\tau_l}\left[\frac{\tau}{\tau_i}(1-e^{-t/\tau})\right]. \end{aligned} \tag{23}$$

The first two terms account for situations where the ion is at l at time 0, and at l or i at later times. The last two terms describe the corresponding situations with the ion at i at time 0.

Spatial Fourier transformation yields the intermediate self-correlation function of silver:

$$F_s^{\mathrm{Ag}}(\boldsymbol{Q},t) = 1 - 2\frac{\tau}{\tau_i\tau_l}(1-\cos(\boldsymbol{Q}\cdot\boldsymbol{x}_0))\cdot(1-e^{-t/\tau}) \tag{24}$$

After directional averaging, $\cos(\boldsymbol{Q}\cdot\boldsymbol{x}_0)$ is replaced by $\sin(Qx_0)/(Qx_0)$. For the quasielastic incoherent scattering function we thus find

$$S_{\mathrm{inc}}^{\mathrm{Ag}}(Q,\omega) = \frac{1}{\pi}\left[1-\frac{\sin(Qx_0)}{Qx_0}\right]\cdot\frac{\tau^2}{\tau_i\tau_l}\cdot\frac{\tau}{1+\omega^2\tau^2}\,, \tag{25}$$

which becomes

$$S_{\mathrm{inc}}^{\mathrm{Ag}}(Q,\omega) = \frac{1}{\pi}\left[1-\frac{\sin(Qx_0)}{Qx_0}\right]\cdot\frac{\tau_i^2}{\tau_l}\cdot\frac{1}{1+\omega^2\tau_i^2}\,, \tag{26}$$

for $\tau_i \ll \tau_l$. According to (26) and (11), the quasielastic scattering is expected to depend on both frequency and temperature in precisely the same way as does $\sigma_{l,i}(\omega)/\omega^2$.

In Figs. 9a, b, c we present our experimental total scattering functions taken at $Q \approx 3.4$ Å^{-1} and at the three temperatures 473 K, 548 K, and 623 K. The spectra contain elastic, quasielastic, and inelastic components. The solid lines have been obtained by superimposing a temperature independent inelastic contribution, a thermally activated quasielastic (Lorentzian) line, and a bit of elastic scattering. The inelastic and quasielastic parts of the spectra are plotted separately

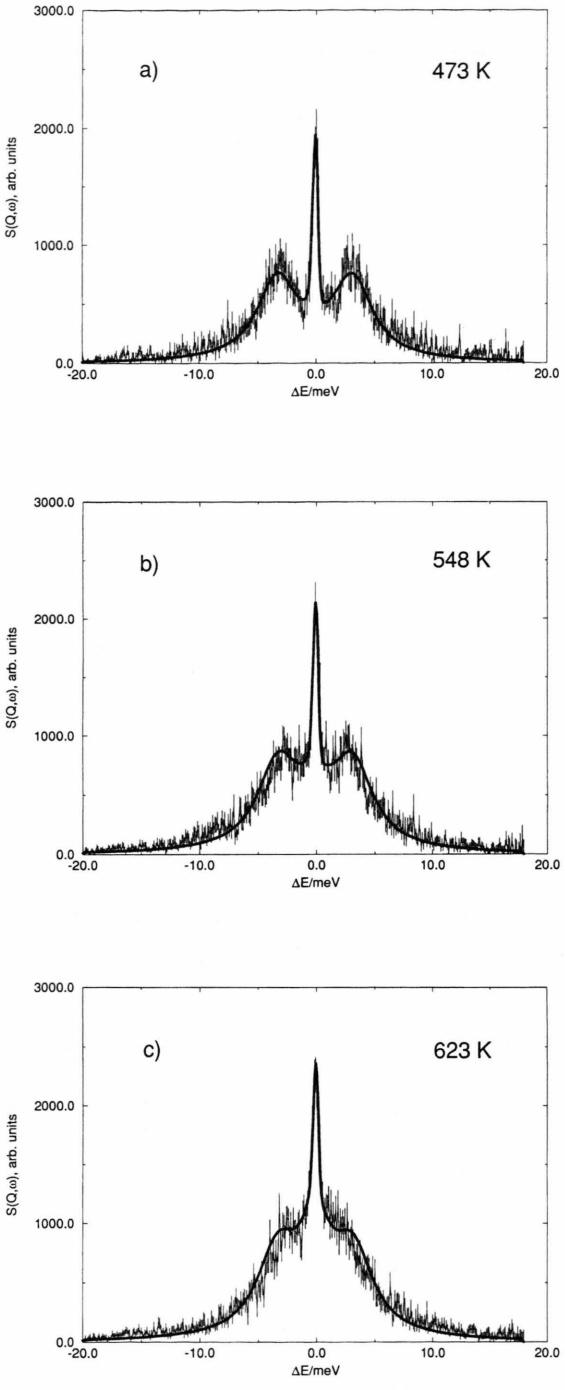

Fig. 9. Experimental total scattering functions of AgBr at $Q \approx 3.4$ Å^{-1} and at a) 473 K, b) 548 K, c) 623 K, as obtained on the neutron-scattering spectrometer MARI. The solid lines are superpositions of the inelastic and quasielastic components shown in Figs. 10a and 10b, and of some purely elastic scattering, convoluted with the experimental resolution function.

in Figs. 10a and 10b. For comparison, the corresponding parts of $(\sigma(\omega)-\sigma(0))/\omega^2$ are displayed in Fig. 10c and 10d.

Not surprisingly, the relative weight of the inelastic component is larger in the neutron scattering spectra than it is in $(\sigma(\omega)-\sigma(0))/\omega^2$, acoustic phonon modes being excited by the $Q \approx 3.4$ Å^{-1} neutrons. The quasielastic components of Figs. 10b and 10d are both thermally activated, with similar activation energies. Moreover, in either case the width does not seem to change with temperature.

Surprisingly, however, we find quite different quasielastic line widths in Figs. 10b and 10d. In contrast to our expectations, the neutron data yield a comparatively large half width at half maximum,

$$\mathrm{HWHM}_n \approx 1.6 \text{ meV}, \tag{27a}$$

while the respective value obtained from $(\sigma(\omega)-\sigma(0))/\omega^2$ is only

$$\mathrm{HWHM}_\sigma \approx 0.65 \text{ meV}. \tag{27b}$$

For an explanation of the observed quasielastic neutron scattering, it is not easily possible to find a generic dynamic process that is quite different from the one considered so far. The view that the quasielastic lines of Figs. 10b and 10d should essentially be due to the same process is corroborated by the close agreement of their respective activation energies. However, using neutrons, this process appears to be faster or to contain faster constituents than expected on the basis of the conductivity data.

In this context, it is important to note that non-periodic displacements of *other* ions, which are causally related to the trial-and-error hopping motion of the *central* ion, but of shorter distance, will show up in the neutron scattering with a much larger weight than in the expression $(\sigma(\omega)-\sigma(0))/\omega^2$. In the incoherent quasielastic scattering, for instance, the weighing factor for displacements of distance $x \leq x_0$ and back again is proportional to $1-\sin(Qx)/(Qx)$, while the respective factor in the expression $(\sigma(\omega)-\sigma(0))/\omega^2$ varies as x^2. Figure 11 is a plot of the two functions.

Furthermore, non-periodic displacements that are causally related to the hopping of the central ion will contribute significant *coherent* quasielastic scattering. This is due to cross terms ($m \neq n$), where m and n denote either another ion and the central ion, or even two other ions. The typical form of a contribution of this kind is

$$S_{m,n}(\boldsymbol{Q},\omega) \propto \mathrm{Re} \int < e^{i\boldsymbol{Q}(\boldsymbol{R}+\boldsymbol{r}_m(t)-\boldsymbol{r}_n(0))} > e^{i\omega t}\, \mathrm{d}t\,. \tag{28}$$

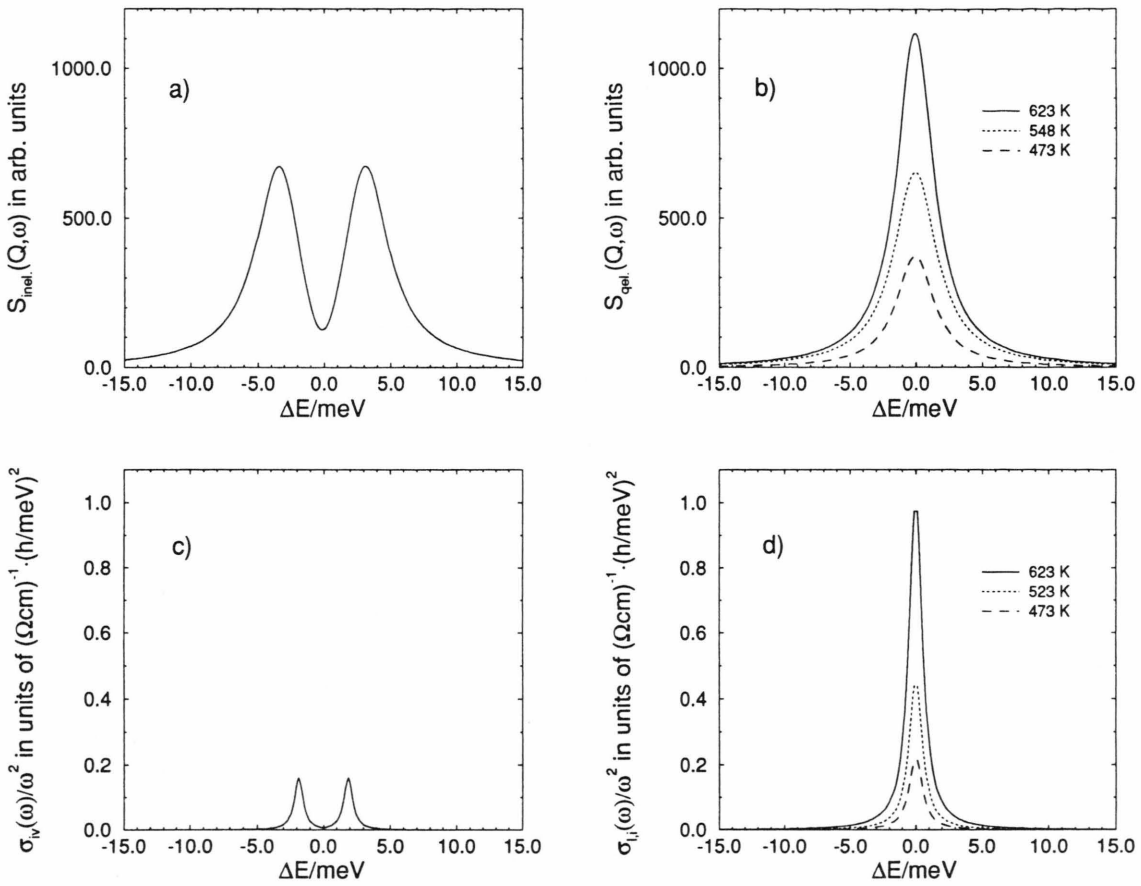

Fig. 10. a) Inelastic and b) quasielastic components of the neutron-scattering spectra of Fig. 9; c) and d) are the respective components detected in $(\sigma(\omega)-\sigma(0))/\omega^2$.

In (28), the vector $\boldsymbol{R}$ connects lattice sites m and n, while $\boldsymbol{r}_m$ and $\boldsymbol{r}_n$ denote the displacements of the respective ions from those sites. If, e.g., one of the ions is the central ion and the other a neighbouring one, then a substantial contribution to the total scattering function will result if the neighbouring ion moves back and forth by a fraction of an Ångstrøm.

We now argue that, in fact, *all* of the six constituent parts of $S^{tot}(Q,\omega)$, as given in (22), will contribute quasielastic intensity, caused by the occurrence of fast cooperative and correlated displacive movements of ions in the immediate neighbourhood of the hopping central ion.

As an example, let us consider the bromide ion located at a distance of $2x_0$ from site l, in the direction of site i, but beyond it. As the central ion hops from l to i and back again, the bromide ion is expected to bounce back and forth in a correlated manner. The *rms* displacement of Br^- being close to 0.4 Å [15], a displacive movement of about 0.5 Å appears very probable. This implies quasielastic contributions by all of the last four terms in (22). In particular, the coherent Ag–Br and Br–Ag cross terms will have similar weight as the term discussed in (26), since the variation of the real part of the expression in brackets in (28), is of the order of one, if Q is 3.4 $Å^{-1}$. Besides these cross terms, the self-correlation of the recoiling motion of the bromide ion will also contribute quasielastic intensity, via the last two parts of (22).

The activation energy of the quasielastic scattering due to correlated displacements of neighbouring ions has to be Δ, as they occur only along with the hopping motion of the central ion. Therefore, quite a number of identically activated quasielastic contributions will

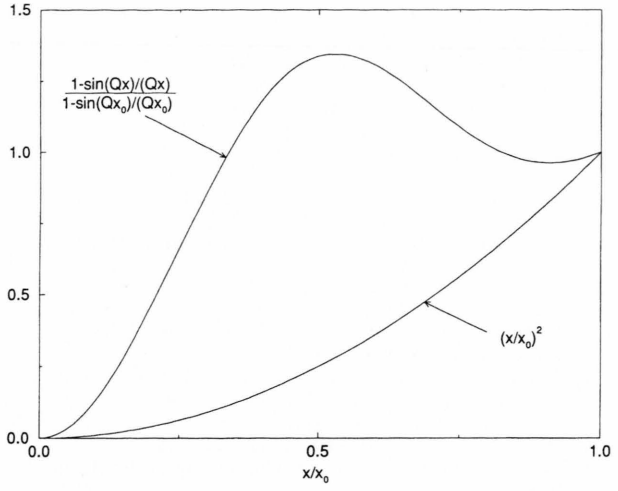

Fig. 11. Weighing factors for incoherent quasielastic scattering and for $(\sigma(\omega)-\sigma(0))/\omega^2$, if the displacement is x instead of x_0. According to (26) and (11), the factors are $[1-\sin(Q\,x)/(Q\,x)]/[1-\sin(Q\,x_0)/(Q\,x_0)]$ and $(x/x_0)^2$, respectively. The numerical values are $Q=3.4\,\text{Å}^{-1}$, and $x_0=2.5$ Å.

be superimposed in the spectrum. Compared with the trial-and-error hopping process of the central ion, the cooperative displacive movements of its neighbours will not only be more localized but also faster. This results in broader quasielastic lines. What we observe, cf. Fig. 10b, is a superposition which is not easy to decompose.

V. Conclusion

The microwave and far-infrared conductivity of solid silver bromide exhibits a pronounced Debye-relaxation-type dispersion, which is consistently explained by the formation and direct recombination of Frenkel pairs. The back-and-forth hopping of silver ions between lattice and neighbouring interstitial sites accounts for the major part of the conductivity at millimetre-wave frequencies and has, therefore, to be considered the most frequent hopping process in AgBr. This statement, together with the observation of high-amplitude vibrational movements of individual silver ions along ⟨111⟩ directions, is in agreement with structural data showing a high Ag^+ probability density between octahedral lattice sites and tetrahedral interstitial sites.

The predominance of cation back-and-forth hopping in AgBr appears to be contradictory to the generally accepted view, which emphasizes the importance of collinear intersticialcy jumps [6]. Of course, these two pictures do not exclude each other; they simply describe dynamic features observed on different time scales.

The localized back-and-forth hopping of individual silver ions is accompanied by cooperative displacive movements of their neighbouring ions. Our quasielastic neutron scattering spectra bear clear evidence of these relatively fast relaxations. At the same time, the relaxation of the surrounding ions accounts for a lowering of the potential energy of the particular (short lived) configuration when the interstitial ion and the vacancy are direct neighbours. Although the vacancy–ion pair will recombine in a vast majority of cases, there is also a possibility for the interstitialcy to be liberated from the vacancy, via a series of collinear interstitial hops. The energy required for this process is considerably enhanced by the relaxation of the neighbourhood and found to be about 0.86 eV.

Acknowledgements

We wish to thank J. Dreyer (RAL sample environment group) and R. S. Eccleston for their kind assistance during the neutron scattering experiment.

The experimental and theoretical analysis of the frequency dependent ionic conductivity was funded by the Deutsche Forschungsgemeinschaft.

Financial aid was provided by the Bundesminister für Forschung und Technologie.

Financial help by the Fonds der Chemischen Industrie is also gratefully acknowledged.

[1] A. L. Laskar, in: A. L. Laskar, S. Chandra, eds., Superionic Solids and Solid Electrolytes, Recent Trends, p. 265, Academic Press, San Diego 1989.
[2] J. Teltow, Ann. Physik **5,** 63 (1949).
[3] R. J. Friauf, Phys. Rev. **105,** 843 (1957).
[4] B. Aghdaie and R. J. Friauf, Bull. Amer. Phys. Soc. **33,** 333 (1988).
[5] K. Aboagye and R. J. Friauf, Phys. Rev. B **11,** 1654 (1975).
[6] R. J. Friauf, in: A. Balderschi, W. Czaja, E. Tosatti, and M. Tosi, eds., The Physics of Latent Image Formation in Silver Halides, p. 79, World Scientific, Singapore 1984.
[7] P. W. M. Jacobs, J. Corish, B. A. Devlin, and C. R. A. Catlow, in: P. Vashishta, J. N. Mundy, G. K. Shenoy, eds., Fast Ion Transport in Solids, p. 589, Elsevier North Holland, New York 1979.
[8] J. Corish and D. C. A. Mulcahy, J. Phys. C: Solid St. Phys. **13,** 6459 (1980).
[9] G. Everett, A. W. Lawson, and G. E. Smith, *Phys. Rev.* **123,** 1589 (1961).
[10] P. Debye and H. Falkenhagen, Physik. Z. **24,** 121 (1928).
[11] P. Debye and H. Falkenhagen, Physik. Z. **24,** 401 (1928).
[12] B. Roling, T. Lauxtermann, and K. Funke, Solid State Ionics **51,** 13 (1992).
[13] A. K. Jonscher, Nature London **267,** 673 (1977).
[14] K. Funke, Prog. Solid St. Chem. **22,** 111 (1993).
[15] D. A. Keen, R. L. McGreevy, W. Hayes, and K. N. Clausen, Philos. Mag. Lett. **61,** 349 (1990).
[16] D. A. Keen, W. Hayes, and R. L. McGreevy, J. Phys.: Cond. Matter **2,** 2773 (1990).
[17] V. M. Nield, D. A. Keen, W. Hayes, and R. L. McGreevy, J. Phys.: Cond. Matter **4,** 6703 (1992).
[18] K. Funke, J. Kümpers, and J. Hermeling, Z. Naturforsch. **43a,** 1094 (1988).
[19] K. Funke, T. Kantimm, and D. Zurwellen, Ber. Bunsenges. Phys. Chem. **93,** 1331 (1989).
[20] R. Hoppe, T. Kloidt, and K. Funke, Ber. Bunsenges. Phys. Chem. **95,** 1025 (1991).
[21] R. Kubo, J. Phys. Soc. Japan **12,** 570 (1957).
[22] W. Bührer, Phys. Stat. Sol. B **68,** 739 (1975).
[23] H. Scher and M. Lax, Phys. Rev. B **7,** 4491 (1973).
[24] H. Schmalzried, Z. Physik. Chem. **22,** 209 (1959).
[25] M. Bée, Quasielastic Neutron Scattering, Adam Hilger, Bristol 1988.